UDC 621.3.015.52: 621.3.022: 621.319.53 https://doi.org/10.20998/2074-272X.2025.4.09

V.F. Bolyukh, G.M. Suchkov, R.P. Mygushchenko, M.E. Kalnytskyi

Determination of parameters of an autonomous source of a constant magnetic field for a portable electromagnetic-acoustic transducer

Purpose. *Determination of rational parameters of an autonomous source of constant magnetic field, ensuring the efficiency of using portable electromagnetic-acoustic transducers (EMAT) for diagnostics of remote ferromagnetic objects.* ***Methodology.*** *An analysis of the parameters of an autonomous magnetic field source consisting of a permanent magnet and a ferromagnetic screen magnetizing a ferromagnetic object with a flat surface, providing a central magnetic field along the magnet axis above 0.3 T, was carried out.* ***Results.*** *The results of experimental studies on a sample of an autonomous source, which contained 6 sections of a permanent magnet made of NeFeB ceramics with dimensions of 50×50×10 mm*^{3}*, correspond to the results of calculating the magnetic field on the surface of a ferromagnetic sample with an error of up to 9 %. Experimental studies were carried out for EMAT with two magnetic field sources containing rectangular permanent magnets of the same height but different widths.* ***Novelty.*** *It has been established that in order to select rational parameters of an autonomous source of magnetic field, it is necessary to use an integral criterion that takes into account the magnetic field in the surface layer of a ferromagnetic object, the magnetic scattering field, the volume of a permanent magnet, which determines the mass and size indicators and cost of the source, and the force of attraction to the ferromagnetic object.* ***Practical value.*** *For portable EMAT, increasing the magnetic field in a remote ferromagnetic object either by increasing the volume of a permanent magnet or by decreasing the air gap between the magnetic field source and the ferromagnetic object provides increased EMAT efficiency by increasing the ratio of the amplitude of the received ultrasonic bottom pulses to the noise amplitude.* References 27, figures 14.
Key words: **autonomous magnetic field source, permanent magnet parameters, magnetic field, remote ferromagnetic object, integral criterion, electromagnetic-acoustic transducer, signal amplitude, noise.**

Мета*. Визначення раціональних параметрів автономного джерела постійного магнітного поля, які забезпечують ефективність використання портативних електромагнітно-акустичних перетворювачів (ЕМАП) для діагностики віддалених феромагнітних об'єктів.* ***Методологія****. Проведено аналіз параметрів автономного джерела магнітного поля, що складається з постійного магніту та феромагнітного екрана, що намагнічує феромагнітний об'єкт з плоскою поверхнею, забезпечуючи центральне магнітне поле вздовж осі магніту понад 0,3 Тл.* ***Результати*** *експериментальних досліджень на зразку автономного джерела, який містив 6 секцій постійного магніту з кераміки NeFeB розмірами 50×50×10 мм*^{3}*, відповідають результатам розрахунку магнітного поля на поверхні феромагнітного зразка з похибкою до 9 %. Експериментальні дослідження були проведені для ЕМАП з двома джерелами магнітного поля, що містять прямокутні постійні магніти однакової висоти, але різної ширини.* ***Новизна****. Встановлено, що для вибору раціональних параметрів автономного джерела магнітного поля необхідно використовувати інтегральний критерій, який враховує магнітне поле в поверхневому шарі феромагнітного об'єкта, магнітне поле розсіювання, об'єм постійного магніту, який визначає масогабаритні показники та вартість джерела, силу притягання до феромагнітного об'єкта.* ***Практична значимість****. Портативний ЕМАП забезпечує збільшення відношення амплітуд інформаційних донних імпульсів до шуму шляхом нарощування об'єму його постійного магніту та зменшення повітряного зазору між джерелом магнітного поля і феромагнітним об'єктом.* Бібл. 27, рис. 14.
Ключові слова: **автономне джерело магнітного поля, параметри постійного магніту, магнітне поле, віддалений феромагнітний об'єкт, інтегральний критерій, електромагнітно-акустичний перетворювач, амплітуда сигналу, шум.**

Introduction. Sources of constant magnetic field (SMF) intended for magnetization of ferromagnetic objects (FO) located at a considerable distance (up to 20–50 mm) are used in various fields of science and technology. Thus, electromagnetic-acoustic transducers (EMAT) are used for monitoring and diagnostics of ferromagnetic products with dielectric coatings or deposits on the surfaces. The coating thickness of the products being monitored can reach up to 5 mm, and deposits, for example, on the internal surfaces of pipelines, up to 20 mm or more. The efficiency of these transducers depends on the degree of magnetization of the FO surface layer, remote from the SMF [1].

The problem of creating a compact and powerful SMF for magnetizing a FO located at a considerable distance from it is relevant for various scientific and technical tasks. Such sources of constant magnetic field are necessary for magnetic separation, nanotechnology, materials science, biomedical diagnostics, etc. [2–7]. At the same time, in many practical applications they must operate autonomously, without using an external power source as part of a portable device performing various tasks, for example, non-destructive testing of ferromagnetic products.

Features of SMF for EMAT. In non-destructive testing of ferromagnetic products, EMATs with SMF are used, which magnetize the product, providing generation of ultrasonic waves using a high-frequency coil [8].

In principle, the EMAT includes a SMF 1 and a flat high-frequency inductance coil 2, which affect the FO 3 (Fig. 1).

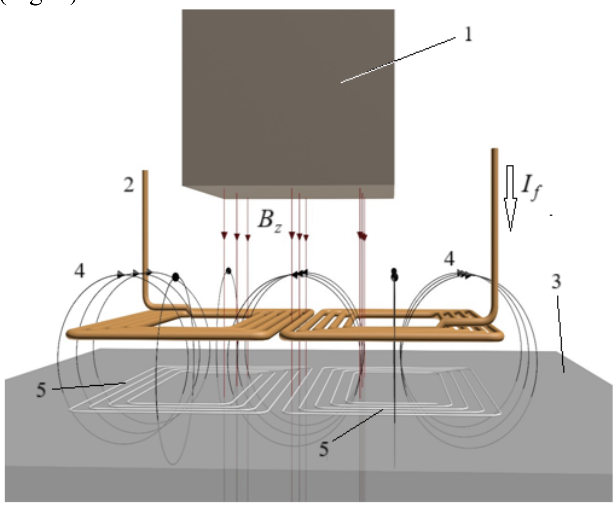

Fig. 1. Scheme of a portable EMAT: 1 – SMF; 2 – inductance coil; 3 – FO; 4 – electromagnetic field; 5 – eddy currents in FO

The SMF forms the normal component of the induction of the constant magnetic field B_z, which acts on the FO. A high-frequency current I_f flows in the inductance coil, which, due to the high-frequency electromagnetic field 4, induces eddy currents 5 in the surface layer of the FO. When the eddy current I_f interacts with the magnetic field B_z, an alternating elastic Lorentz force acts on the conduction electrons, which is transmitted to the crystal lattice of the FO. As a result, ultrasonic pulses with a frequency f are excited. Eddy currents in the FO, due to elastic oscillations of the crystal lattice, induce an alternating current with a frequency f in the inductance coil 2, which acts as a receiver of ultrasonic pulses.

Thus, for diagnostics of a steel pipe, an EMAT is used, containing an SMF of four permanent magnets (PM), the same poles of which are separated by an angle in the range from 30° to 60° [9]. This SMF provides better homogeneity of the magnetic field in the surface layer of the FO compared to configurations of two poles facing each other or quadrupole geometry.

To generate ultrasonic waves in the FO, SMFs with a periodic PM configuration are used in EMAT [10]. Compared to a single PM, a periodic configuration of magnets increases the maximum induction, providing the required value and distribution pattern on the FO surface, especially under the coil generating high-frequency signals [11]. To increase the magnetic field in the FO, both various magnetic concentrators [12] and several PMs, such as Halbach magnet configurations [13], are proposed.

A mobile robotic system designed to create internal maps of the investigated FO and its structural elements uses a movable EMAT. One of the main tasks of such a system was the selection of PM parameters that take into account the required magnetization of the FO and the mass and dimensional parameters of the converter [14].

Problems arise during operation of PM due to elevated temperatures and irreversible demagnetization [15]. The degree of recovery of irreversible demagnetization of PM depends on the choice of magnetic material and the configuration of the system, including the geometry of the magnet, its interaction with other ferromagnetic materials and magnetic fields [16]. As an alternative to PM, long-acting electromagnets or pulsed electromagnets are used, but their operation requires external power sources [17, 18].

When magnetizing the FO from an autonomous SMF, an attractive force arises between them, which must be taken into account, especially when the source is used in portable devices. Between cylindrical PM and FO, this force is directly proportional to the residual magnetic field of magnetization, the cross-sectional area of the PM, the saturation magnetic field and the cross-sectional area of the FO, and inversely proportional to the square of the distance between them [19].

When testing a FO using an EMAT that uses overhead SMFs, it is necessary to know the distribution of the magnetic flux in the surface and internal layers of the object being tested [20]. The gap between the SMF and the FO changes the spatial distribution of the field inside the tested object. Changing the gap under one of the magnets affects the distribution of the magnetic field in the entire volume of the tested FO, and not only in the area located with a gap under this magnet.

By increasing the size of the autonomous SMF to a certain level, a significant increase in the EMAT performance is ensured. However, with an excessive increase in the size of the source, the efficiency of the converter increases insignificantly, and the weight and size parameters become too large, which is unacceptable for a portable device [21].

As is known, the efficiency of EMAT, diagnosing a remote FO, is estimated by the conversion coefficient [22]:

$$\eta = k \cdot I_f \cdot B_z^2 \cdot \exp(-h/R),$$

where k is a coefficient depending on the electrical, magnetic and elastic characteristics of the FO material; I_f is the high-frequency current in the induction coil with an average radius R; B_z is the value of the normal component of the induction of the constant magnetic field in the surface layer of the FO; h is the distance from the SMF to the FO.

The efficiency of EMAT can be increased by both increasing the current I_f in the high-frequency coil and increasing the magnetic field induction B_z in the surface layer of the FO. Since the efficiency of EMAT depends to a greater extent on the value of B_z than on I_f, this necessitates an increase in the induction of the constant magnetic field in the surface layer of the FO to increase the efficiency of EMAT [1].

Thus, the autonomous SMF of a portable EMAT should maximally magnetize the FO located at a significant distance from it (up to 50 mm).

Despite the significant amount of research on the development of EMAT, the problem of choosing rational parameters of an autonomous SMF, taking into account the main indicators, remains unresolved. These are the magnetization level of the remote FO, the dimensions of the PM, which affect the weight and size indicators and the cost of the device, the force of attraction to the FO and the scattering field, which is important when operating the converter [23].

The **purpose** of the article is to determine the rational parameters of an autonomous source of a constant magnetic field, ensuring the efficiency of using portable EMATs for diagnostics of remote ferromagnetic objects with a flat surface.

Research object. Let us consider an autonomous SMF as part of a portable EMAT. The SMF consists of a PM 1 and a ferromagnetic screen (FS) 2, coaxially installed on the upper end of the PM (Fig. 2). The lower end of the PM faces the flat outer surface of the FO 3, which is of considerable length and thickness. The autonomous SMF is located at a considerable distance from the FO, so that between the lower end of the PM and the outer surface of the FO there is an air gap of height Z_1, in which a high-frequency inductance coil 4 is installed. Figure 2 shows the boundary for calculating the average value of the magnetic leakage field B_{ex} 5 and the central axis of the magnetic system 6, coinciding with the z axis of the Cartesian coordinate system.

PM based on NeFeB ceramics with a coercive force of 1114 kA/m [24] is made in the form of a square with a side a and a height H_1 with axial magnetization. FS is made of St10 steel in the form of a disk with a square cross-section and a height h_e.

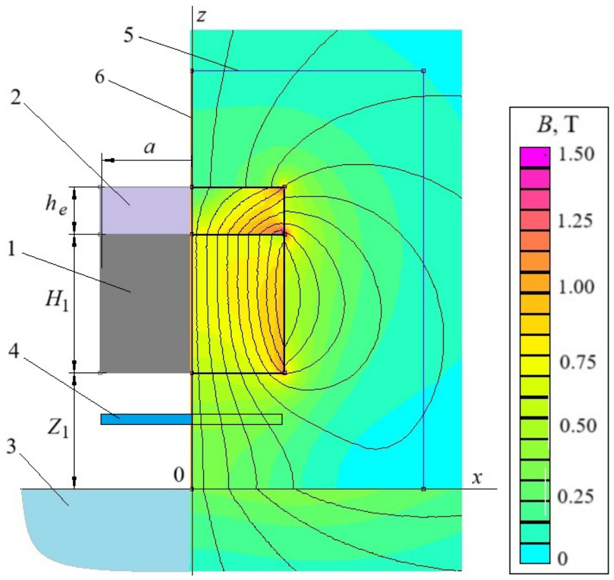

Fig. 2. Schematic diagram of an autonomous SMF as part of a portable EMAT (to the left of the 0z axis) and the distribution of the magnetic field it creates (to the right of the 0z axis):
1 – PM; 2 – FS; 3 – FO; 4 – inductance coil;
5 – calculation limit B_{ex}; 6 – central axis of the magnetic system

Influence of geometric parameters on SMF indicators. Let us consider an autonomous SMF with a permanent magnet intended for EMAT. The magnetic field analysis will be performed in the plane ($z0x$) passing through the central axis of the magnetic system. The magnetic system is calculated using known mathematical expressions using the FEMM program **[**25]. This program solves a large system of algebraic equations, which are formed based on the finite element method and a differential equation describing the magnetic field in the cross section of a magnetic system.

Autonomous SMF should magnetize FO so that the central magnetic field B_0 – magnetic field along the axis of magnetic system 6 in its surface layer (Fig. 2) was above $B_{\min}$=0.3 T. Such a field is necessary for portable ultrasonic EMAT devices when performing thickness measurement and diagnostics of ferromagnetic products. PM is located at a distance of Z_1=25 mm from FO and its width a should not exceed 80 mm, which is important for portable EMAT. FS has the same cross-section as PM, and its height h_e=10 mm.

We will calculate the average value of the magnetic stray field B_{ex} at boundary 5, located at a distance of 25 mm from the outer boundary of the autonomous SMF.

Based on previous studies [1], we select the basic version of an autonomous source with the PM parameters: the square side a=30 mm, the height H_1=40 mm. This SMF at Z_1=25 mm magnetizes the FO to the minimum required value B_0=$B_{\min}$ (more precisely B_0=0.299 T). In this case, the magnetic stray field B_{ex}=0.106 T, and the source is acted upon by an axial attractive force F_z =37.44 N from the FO side. Figure 2 shows the lines of force and the induction of the magnetic field created by the basic version of the SMF during magnetization of the remote FO.

Let us consider the influence of the parameters of the autonomous SMF on the magnetic field in the surface layer of the FO (along the 0x axis). With an increase in the height of the PM H_1 and an unchanged cross-section with a side of a=50 mm, the maximum magnetic field in it increases (Fig. 3). The greatest value of the field occurs inside the PM. However, in the FO, the magnetic field also increases both in magnitude and in the area of influence.

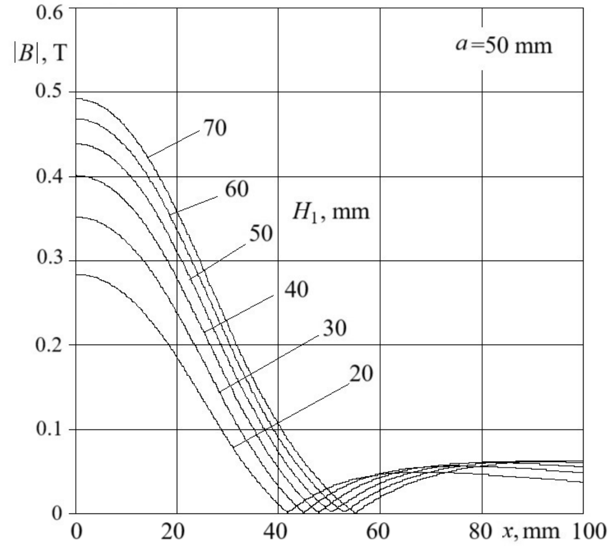

Fig. 3. Distribution of the magnetic field induction modulus in the surface layer of the FO at different PM heights

If the PM is made of a small height (H_1=20 mm), then the required value of the central field $B_{\min}$ on the surface of the FO is not ensured. With a linear increase in the height of the PM, the magnetic field in the FO increases nonlinearly with a decrease. This shows the inexpediency of increasing the height of the PM above a certain value.

A more appropriate way to increase the magnetic field in the FO is to increase the PM width (Fig. 4). In this case, both the central field B_0 and the width of the magnetization region increase in the surface layer of the FO. When the PM width is increased by 2 times from 30 to 60 mm, the central field increases by 1.33 times, and the magnetization area of the FO by a field higher than $B_{\min}$ increases by more than 10 times.

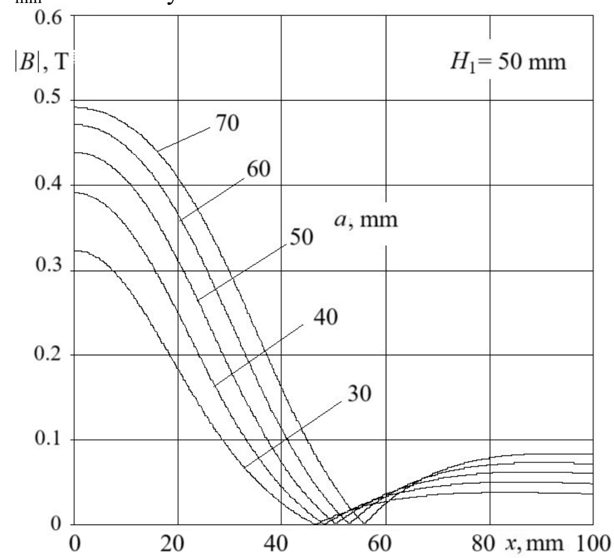

Fig. 4. Distribution of the magnetic field induction modulus in the surface layer of the FO at different PM widths

Figure 5 shows the dependence of the relative values of the central magnetic field B_0^* in the FO (relative to the basic version of the SMF) on the geometric parameters of the PM. With an increase in the volume of the PM, this field also increases, but with a nonlinear decrease in growth. Even with a significant increase in the dimensions of the PM, the central magnetic field increases no more than 2 times relative to the basic version of the SMF. In this case, it is possible to determine the geometric parameters of the PM that provide a magnetic field higher than B_{min} and the magnetization area of the FO by such a field.

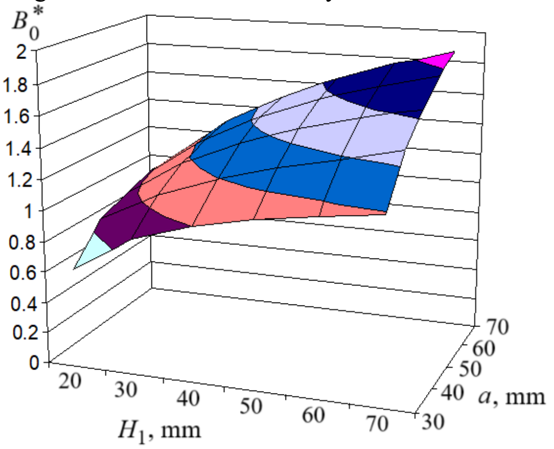

Fig. 5. Dependence of the relative value of the central magnetic field in the FO on the geometric parameters of the PM

However, for a portable EMAT, when selecting the geometric parameters of the PM, in addition to the magnetization field FO, it is necessary to take into account other indicators. These are the magnetic scattering field B_{ex}, the volume of the autonomous source V and the force of attraction of the autonomous source to the FO F_z. The magnetic scattering field B_{ex} has a negative effect on both the nearby electronic system of the device and on the service personnel [26].

The volume V determines the mass, dimensions and cost of the autonomous SMF. The cost is mainly determined by the high-coercivity PM. The attractive force to the FO F_z determines the operating conditions of the portable EMAT. This force is calculated using the well-known formula:

$$F_z = \frac{1}{\mu_0} \oint_S 2\pi r (B_r \cdot B_z) \mathrm{d}S ,$$

where B_r, B_z are the radial and axial components of the magnetic field induction in the volume of the SMF covered by the surface S.

Figure 6 shows the force of attraction of the SMF to the FO F_z^* in relative form.

As follows from the presented graph, with an increase in the volume of the PM V (height H_1 or width a), the attractive force increases. If the width of the PM is insignificant (a=30 mm), then the force from the height of the PM increases insignificantly. With the maximum parameters of the PM from the considered range (H_1=a=70 mm), this force increases almost 14 times compared to the basic version of the SMF.

As calculations show, the nature of the change in the magnetic field scattering B_{ex} into the surrounding space depending on the geometric parameters of the PM largely corresponds to the nature of the change in the central magnetic field B_0 in the FO.

Since with the increase in the volume of PM V all the indicators of SMF increase, the question arises about the nature of these indicators with the same volume, but a different combination of height H_1 and width a.

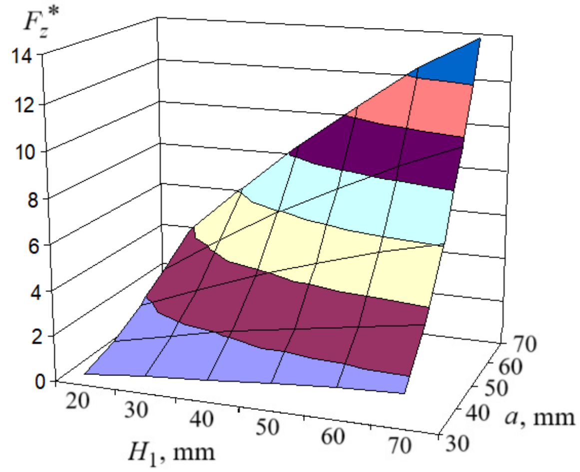

Fig. 6. Dependence of the relative values of the force of attraction of the SMF to the FO on the geometric parameters of the PM

Figure 7 shows the dependence of the relative SMF indicators on the width a for a small (V=125·10^3 mm^3) and large (V=216·10^3 mm^3) volume of the PM. The small value of V is due to the choice of the basic version of the PM with parameters H_1=a=50 mm, and the large value of V is due to the choice of the basic version of the PM with parameters H_1=a=60 mm.

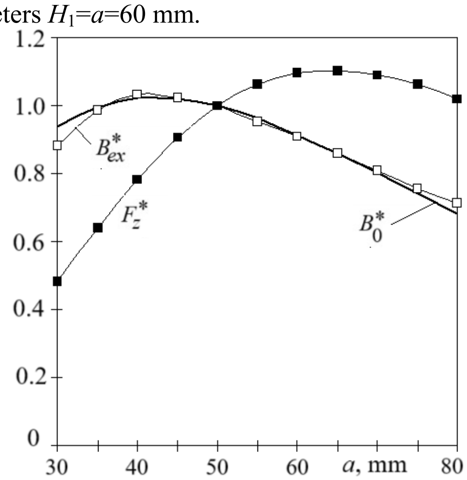

a

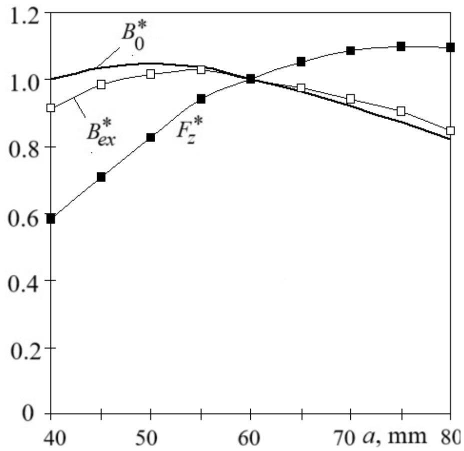

b

Fig. 7. Dependence of relative SMF indicators on the width of the PM for a small (*a*) and large (*b*) volume V

With a constant PM volume, the maximum value of the central field B_0 in the FO occurs at a certain width. For a PM with a small volume, this is approximately a=40 mm, and for a PM with a large volume, this is approximately a=50 mm. Note that these dimensions are smaller than the width of the base PM. The nature of the scattering field B_{ex} largely corresponds to the central field B_0.

The nature of the force of attraction of F_z SMF to FO is different. The maximum force occurs when the width of the magnet is greater than the base one. For PM with a small volume, this is approximately a=65 mm, and for PM with a large volume, a=75 mm.

Let us consider the influence of the height FS he on the SMF indices (Fig. 8). This screen slightly (up to 4 %) increases the central magnetic field in the FO B_0. As a result, the force of attraction of the SMF to the FO F_z increases to a greater extent (up to 8 %). At the same time, the magnetic field of scattering into the surrounding space B_{ex} decreases, but slightly (up to 3 %).

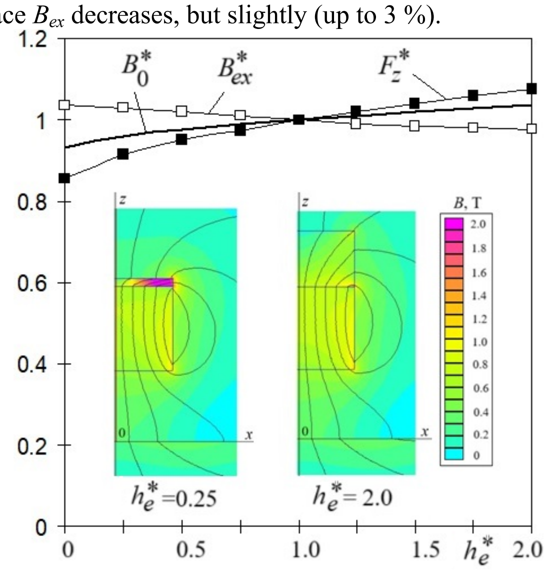

Fig. 8. Dependence of relative SMF indicators on the height of the ferromagnetic shield

The highest value of the scattering field B_{ex} occurs in the absence of FS, and the highest central field B_0 occurs at its maximum height. Note that the location of FS on the lateral sides of the PM is inappropriate, since such a design reduces the central magnetic field in the FO with a large air gap Z_1 [1].

Considering that increasing the height of the FS leads to an increase in the height and weight of the autonomous SMF, it can be assumed that the SMF variant with h_e=10 mm, like the basic variant, is acceptable.

Thus, with an increase in the height H_1 and the width a PM, all SMF indicators increase, although to varying degrees. However, an increase in the central magnetic field B_0 in the FO is a positive indicator of an autonomous source, reflecting its main purpose, and an increase in the remaining indicators are negative factors.

Based on the above, the parameters of the autonomous SMF, namely the geometric dimensions of the PM, must be selected taking into account both the positive indicator (the central magnetic field B_0 in the FO) and the negative indicators (the scattering magnetic field B_{ex}, the volume of the SMF V and the force of its attraction to the FO F_z).

The task of selecting the geometric parameters of the PM can be considered as multicriterial. For this purpose, we will reduce the above SMF indicators to one integral criterion using the scalarization function – the canonical additive-multiplicative objective function:

$$K^* = \beta\left(\alpha_1 B_0^* + \frac{\alpha_2}{V^*} + \frac{\alpha_3}{F_z^*} + \frac{\alpha_4}{B_{ex}^*}\right) + (1-\beta)\times$$
$$\times\left(B_0^*\right)^{\alpha_1}\left(\frac{1}{V^*}\right)^{\alpha_2}\left(\frac{1}{F_z^*}\right)^{\alpha_3}\left(\frac{1}{B_{ex}^*}\right)^{\alpha_4}, \quad \sum_{i=1}^{4}\alpha_i = 1,$$

where α_i are the weight coefficients of the objective function; β is the empirical coefficient.

Based on expert assessments, we set the coefficients α_1=0.5; α_2=0.2; α_3=0.2; α_4=0,1; β=0.75. The integral efficiency criterion from the geometric parameters of the PM of an autonomous SMF is presented in Fig. 9.

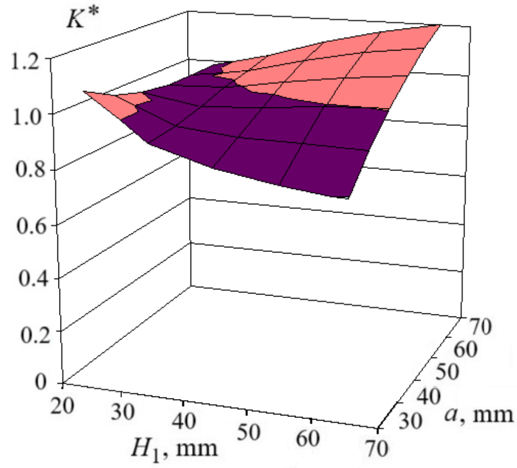

Fig. 9. Dependence of the integral criterion of SMF efficiency on the geometric parameters of the PM

Based on the obtained dependencies, it can be concluded that the most effective are SMFs, in which the PM have the largest width and height from the considered range. This is due to the fact that such magnets magnetize the FO more strongly. However, PMs with a small width and height can also be quite effective, provided that their central field value B_0>B_{min}. Such SMFs have small mass-dimensional parameters and a relatively low cost.

Experimental studies. For experimental verification of the magnetic field modeling results, a sample of an autonomous SMF was manufactured, providing magnetization of a remote FO (Fig. 10). This sample contained 6 flat PM sections with dimensions of 50×50×10 mm^3 each made of NeFeB ceramics. The sections were arranged in a column so that the PM height was 60 mm. On top of the PM there was an FS with dimensions of 50×50×10 mm^3, made of St10 steel.

An experimental sample made of St45 steel with dimensions of 180×65×30 mm^3 was used as the FO, on the surface of which measuring paper with divisions of 1 mm was applied (to control the movement step of the Hall sensor, which provided measurement of the axial component of the magnetic field induction B_z at a height of 0.5 mm above the surface of the FO). The measurement of the magnetic field induction value was performed using a pre-calibrated F4354/1 teslameter.

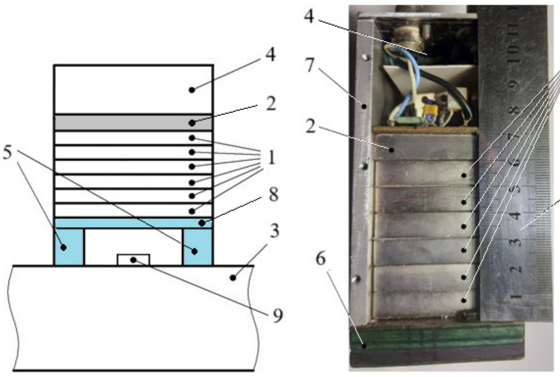

a *b*

Fig. 10. Scheme (a) and experimental sample (b) of an autonomous SMF that provides magnetization of a remote FO: 1 – PM sections; 2 – FS; 3 – FO; 4 – electronic unit; 5 – insulating supports of variable height; 6 – dielectric pads; 7 – housing; 8 – insulating protector; 9 – Hall sensor; 10 – measuring ruler

A sample of an autonomous small-sized SMF was installed on the FO with a non-magnetic gap Z_1=25 mm (the total height of the insulating supports 5 and the protector 8). The axial component of the magnetic field induction B_z was measured by a Hall sensor on the FO surface every 5 mm from the center at a distance of up to 40 mm along the long side of the experimental steel sample. The measurement results are shown in Fig. 11. In the presented distribution of the magnetic field, the FO is outlined by a contour below the 0*x* axis.

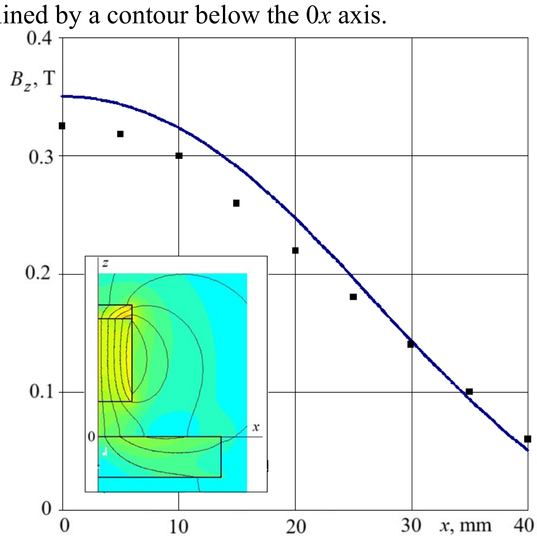

Fig. 11. Results of experimental (points) and calculated (line) values of the axial component of the magnetic field induction B_z and the distribution of the magnetic field for the experimental sample

The experimental data correspond to the simulation results with an error of up to 9 %, which indicates the reliability of the results obtained. The difference between the experimental results and the calculated ones is due to the spread of the parameters of the PM sections due to the manufacturing technology, as well as errors in the location of the Hall sensor relative to the FO.

Practical implementation. Let us consider the use of an autonomous SMF for a portable EMAT, providing excitation and reception of ultrasonic pulses in the FO. Figure 12 shows the diagram and layout of the converter of electromagnetic energy into ultrasonic energy [27] with an autonomous SMF and a system for measuring the distribution of the magnetic field on the surface of the FO.

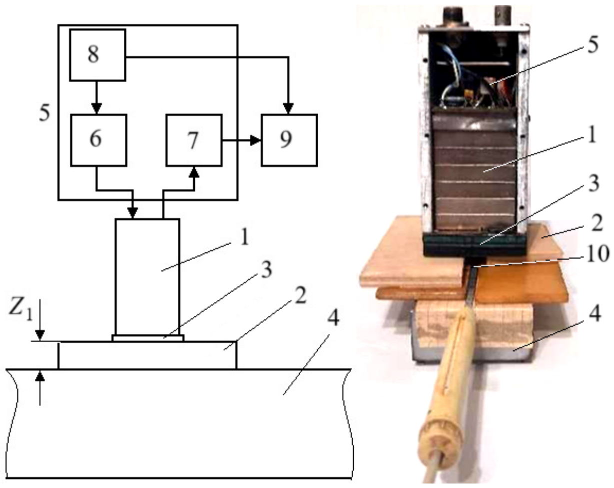

a *b*

Fig. 12. Scheme (a) and layout (b) of EMAP: 1 – SMF; 2 – gaskets; 3 – plate 3 with an inductance coil; 4 – FO; 5 – electronic unit; 6 – pulse generator; 7 – amplifier; 8 – synchronizer; 9 – oscilloscope; 10 – Hall sensor

The converter includes a DPMP 1, dielectric spacers 2 of adjustable height, a dielectric plate 3 with a built-in high-frequency inductance coil, a FO 4, an electronic unit 5 with a high-frequency current pulse generator 6, an amplifier of received ultrasonic pulses 7 and a synchronizer 8. A digital oscilloscope 9 records ultrasonic pulse signals in the FO, and a Hall sensor 10 measures the axial component of the magnetic field on the FO surface.

The converter was installed on the surface of the FO through dielectric spacers of different thicknesses. The efficiency of the SMF was estimated by the amplitude of the received ultrasonic pulses using a SmartDS7202 oscilloscope [8].

Studies were conducted for EMAT with two magnetic field sources: SMF-1 contained 6 PM sections with dimensions of 50×50×10 mm^3, SMF-2 contained 4 PM sections with dimensions of 30×30×15 mm^3. Both sources contained FS with a height of 10 mm. These sources have the same axial height H_1=60 mm, but different PM volumes. SMF-1 has V=150·10^3 mm^3, and SMF-2 has V=54·10^3 mm^3.

Figure 13 shows the time sweeps of the ultrasonic pulses reflected in the FO volume, obtained at different gaps between SMF-1 and the FO surface.

The oscillograms show the probing 1 and the sequence of short bottom 2 ultrasonic pulses reflected in the FO volume.

With a non-magnetic gap between SMF-1 and FO Z_1=25 mm, when the value of the central magnetic field in FO B_0=0.44 T, the amplitudes of the bottom pulses in relation to the noise are at least 10/1, which is sufficient for thickness measurement of ferromagnetic products. With a two-fold decrease in the gap Z_1=12.5 mm, and therefore an increase in the central field to B_0=0.85 T, the amplitudes of the bottom pulses in relation to the noise increase to 30/1, which is applicable for monitoring and diagnostics of ferromagnetic products.

Thus, due to the increase in the magnetic field in the FO, the ratio of the amplitude of the first reflected ultrasonic pulse to the noise amplitude increases by 3 times, which makes it possible to increase the efficiency of EMAT.

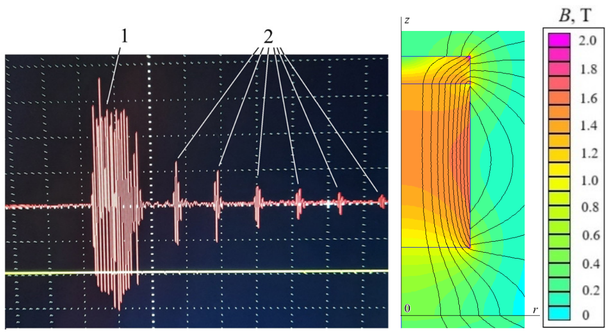

a

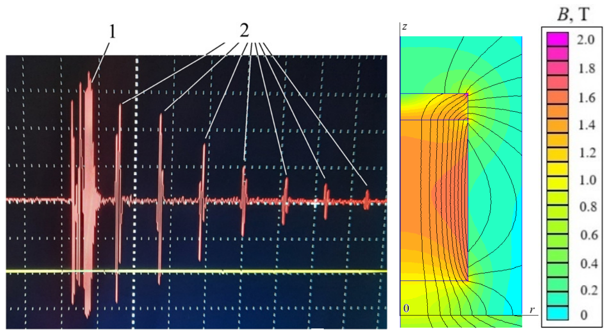

b

Fig. 13. Oscillograms of the sequence of bottom ultrasonic pulses reflected in the FO volume (left) and magnetic field induction (right) at Z_1: 25 mm (*a*) and 12.5 mm (*b*), obtained using SMF-1: 1 – probing pulse; 2 – bottom pulses.

Figure 14 shows the time sweeps of the ultrasonic pulses reflected in the volume of the FO, obtained with similar gaps between SMF-2 and the surface of the FO and the same magnitude of the probing ultrasonic pulse, as when using SMF-1. These oscillograms, as in Fig. 13, show the probing pulse and a sequence of short bottom pulses.

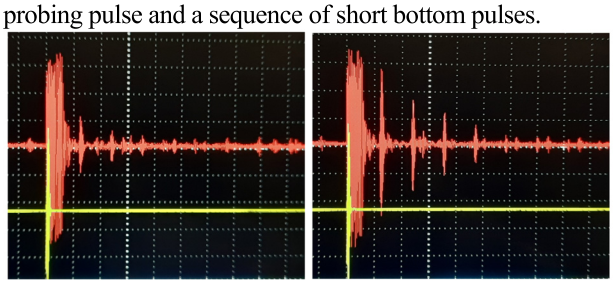

a *b*

Fig. 14. Oscillograms of the sequence of bottom ultrasonic pulses reflected in the FO volume at Z_1: 25 mm (*a*) and 12.5 mm (*b*), obtained using SMF-2

With a non-magnetic gap between SMF-2 and FO Z_1=25 mm (B_0=0.34 T), the amplitudes of the bottom pulses in relation to the noise are 5/1, and when the gap Z_1 is reduced by half, the central magnetic field increases to B_0=0.61 T, which increases the ratio of the amplitude of the bottom pulses to the noise to 13.5/1.

When using SMF-2, which has a PM volume that is almost 3 times smaller than SMF-1, the EMAT efficiency decreases (Fig. 13). This is due to the fact that the amplitudes of short bottom pulses reflected in the FO volume decrease, and their sequence attenuates faster. This indicates the influence of the SMF magnetic field on the EMAT efficiency.

Thus, it has been experimentally confirmed that increasing the magnetic field in the FO by a source with permanent magnets with rational parameters increases the efficiency of EMAT.

In the future, it is advisable to consider the use of either a pulsed electromagnet or the joint use of a pulsed electromagnet and a permanent magnet to amplify and regulate the magnitude of the magnetic field in the surface layer of the FO.

Conclusions.

1. As a result of the analysis of literary sources, the need to select rational parameters for a source of a constant magnetic field that magnetizes a ferromagnetic object when converting electromagnetic energy into ultrasonic energy was established.
2. An analysis was carried out of the parameters of an autonomous source of magnetic field, consisting of a PM and a ferromagnetic screen, which acts on the flat surface of a remote ferromagnetic object, magnetizing it to a given level.
3. It has been established that in order to select rational parameters of an autonomous SMF, it is necessary to use an integral criterion that takes into account the magnetic field in the surface layer of the FO, the magnetic scattering field, the volume of the PM, which determines the mass-dimensional indicators and cost of the SMF, and the force of attraction to the FO.
4. The results of experimental studies on a sample of an autonomous source, which contained 6 sections of PM made of NeFeB ceramics with dimensions of 50×50×10 mm^3, correspond with an error of up to 9 % to the results of calculating the magnetic field on the surface of a ferromagnetic sample made of St45 steel with a thickness of 40 mm.
5. For a portable electromagnetic-acoustic transducer, increasing the magnetic field in the FO either due to the dimensions of the PM or due to a decrease in the air gap between the SMF and the FO provides an increase in the efficiency of the EMAP, increasing the ratio of the amplitude of the bottom pulses to the amplitude of the noise.

Conflict of interest. The authors declare that they have no conflicts of interest

REFERENCES

1. Suchkov G.M., Bolyukh V.F., Kocherga A.I., Mygushchenko R.P., Kropachek O.Y. Increasing the efficiency of the surface-mounted ultrasonic electromagnetic-acoustic transducer on account of the magnetic field source. *Tekhnichna Elektrodynamika*, 2023, no. 2, pp. 3-8. doi: https://doi.org/10.15407/techned2023.02.003.

2. Khalil Baqer Z., Hliyil Hafiz M., Sayyid F.F. Processing of Hematite Ore by using Magnetizing Reduction Roasting and Magnetic Separation. *Salud, Ciencia y Tecnología – Serie de Conferencias*, 2024, vol. 3, art. no. 832. doi: https://doi.org/10.56294/sctconf2024832.

3. Tan Y.W., Leong S.S., Lim J., Yeoh W.M., Toh P.Y. Low-gradient magnetic separation of magnetic nanoparticles under continuous flow: Experimental study, transport mechanism and mathematical modelling. *Electrophoresis*, 2022, vol. 43, no. 21-22, pp. 2234-2249. doi: https://doi.org/10.1002/elps.202200078.

4. Ciannella S., Wu X., González-Fernández C., Rezaei B., Strayer J., Choe H., Wu K., Chalmers J., Gomez-Pastora J. Kinetic and Parametric Analysis of the Separation of Ultra-Small, Aqueous Superparamagnetic Iron Oxide Nanoparticle Suspensions under Quadrupole Magnetic Fields. *Micromachines*, 2023, vol. 14, no. 11, art. no. 2107. doi: https://doi.org/10.3390/mi14112107.

5. Riaz W., Liu Z., Wang X., Shen Y., Farooq O., He C., Shen G. Comparative analysis of electromagnet and coil-based magneto-acoustic emission detection in pre-stressed Q235 steel. *NDT & E International*, 2025, vol. 155, art. no. 103414. doi: https://doi.org/10.1016/j.ndteint.2025.103414.

6. Wang F., Tang D., Gao L., Dai H., Wang P., Gong Z. Magnetic entrainment mechanism of multi-type intergrowth particles for Low-Intensity magnetic separation based on a multiphysics model. *Minerals Engineering*, 2020, vol. 149, art. no. 106264. doi: https://doi.org/10.1016/j.mineng.2020.106264.

7. Kosse J.J., Wessel W.A.J., Zhou C., Dhallé M., Tomás G., Krooshoop H.J.G., Ter Brake H.J.M., Ten Kate H.H.J. Mechanical design of a superconducting demonstrator for magnetic density separation. *Superconductor Science and Technology*, 2021, vol. 34, no. 11, art. no. 115019. doi: https://doi.org/10.1088/1361-6668/ac2c0f.

8. Migushchenko R.P., Suchkov G.M., Petrishchev O.N., Bolyukh V.F., Plesnetsov S.Y., Kocherga A.I. Information-measuring electromechanical transducers for assessing the quality of the surface of ferromagnetic metal items by ultrasonic waves Rayleigh. *Technical Electrodynamics*, 2017, no. 2, pp. 70-76. doi: https://doi.org/10.15407/techned2017.02.070.

9. Pham H.Q., Le V.S., Vu M.H., Doan D.T., Tran Q.H. Design of a lightweight magnetizer to enable a portable circumferential magnetic flux leakage detection system. *Review of Scientific Instruments*, 2019, vol. 90, no. 7, art. no. 074705. doi: https://doi.org/10.1063/1.5090938.

10. Huang X., Xie Y., Liu F., Li J., Jiang W., Huang P., Sun H., Liang H., He S., Hao W., Xu L. A Hybrid Denoising Method for Electromagnetic Acoustic Detection. *IEEE Sensors Journal*, 2024, vol. 24, no. 16, pp. 25523-25530. doi: https://doi.org/10.1109/JSEN.2024.3416161.

11. Gautam A.K., Yin C.-C., Bhattacharya B. A new chevron electromagnetic acoustic transducer design for generating shear horizontal guided wave. *Ultrasonics*, 2023, vol. 135, art. no. 107137. doi: https://doi.org/10.1016/j.ultras.2023.107137.

12. Liu Z., Deng L., Zhang Y., Li A., Wu B., He C. Development of a mode-tuning magnetic-concentrator-type electromagnetic acoustic transducer. *Ultrasonics*, 2020, vol. 103, art. no. 106094. doi: https://doi.org/10.1016/j.ultras.2020.106094.

13. Zhang T., Yang X., Li M., Peng H., Peng W. Enhancing unilateral EMAT performance through topological optimization of Halbach permanent Magnet arrays. *NDT & E International*, 2024, vol. 146, art. no. 103172. doi: https://doi.org/10.1016/j.ndteint.2024.103172.

14. McMillan R., Hampson R., Tabatabaeipour M., Jackson W., Zhang D., Tzaferis K., Dobie G. Design and Manufacture of an Optimised Side-Shifted PPM EMAT Array for Use in Mobile Robotic Localisation. *Sensors*, 2023, vol. 23, no. 4, art. no. 2012. doi: https://doi.org/10.3390/s23042012.

15. Mudapaka V., Garewal P., Gantala T., Balasubramanian K. Design of a Permanent Magnet Electromagnetic Acoustic Transducer (EMAT) for In-Situ Inspection of Metals at high Temperatures. *Proceedings of the 11th European Workshop on Structural Health Monitoring (EWSHM 2024), e-Journal of Nondestructive Testing*, 2024, vol. 29, no. 7. doi: https://doi.org/10.58286/29803.

16. Suresh N., Elliott P., Radu C., Corcoran J. The design of high temperature EMATs to avoid irreversible magnetic losses. *NDT & E International*, 2025, vol. 150, art. no. 103279. doi: https://doi.org/10.1016/j.ndteint.2024.103279.

17. Huo Z., Cai D., Liu D., Duan Y., Meng H., Liu S., Liu X. Development of an electromagnetic bulk wave EMAT. *Journal of Physics: Conference Series*, 2023, vol. 2674, no. 1, art. no. 012012. doi: https://doi.org/10.1088/1742-6596/2674/1/012012.

18. Bolyukh V.F., Katkov I.I. Influence of the Form of Pulse of Excitation on the Speed and Power Parameters of the Linear Pulse Electromechanical Converter of the Induction Type. *Proceedings of the ASME 2019 International Mechanical Engineering Congress and Exposition. Volume 2B: Advanced Manufacturing*, 2019, V02BT02A047. doi: https://doi.org/10.1115/IMECE2019-10388.

19. Hyun D., Shin A. Quantitative Approach to the Magnetic Force of a Cylindrical Permanent Magnet Acting on a Ferromagnetic Object. *New Physics: Sae Mulli*, 2018, vol. 68, no. 11, pp. 1249-1261. doi: https://doi.org/10.3938/NPSM.68.1249.

20. Liu Z., Riaz W., Shen Y., Wang X., He C., Shen G. Magneto acoustic emission technique: A review of methodology, applications, and future prospects in non-destructive testing. *NDT & E International*, 2024, vol. 146, art. no. 103171. doi: https://doi.org/10.1016/j.ndteint.2024.103171.

21. Mirkhani K., Chaggares C., Masterson C., Jastrzebski M., Dusatko T., Sinclair A., Shapoorabadi R.J., Konrad A., Papini M. Optimal design of EMAT transmitters. *NDT & E International*, 2004, vol. 37, no. 3, pp. 181-193. doi: https://doi.org/10.1016/j.ndteint.2003.09.005.

22. Liu C., Li Q., Liu J., Guo A. Influence of coil structure on the distribution of transmitting magnetic field in downhole electromagnetic detection. *2024 6th International Conference on Intelligent Control, Measurement and Signal Processing (ICMSP)*, 2024, pp. 417-420. doi: https://doi.org/10.1109/ICMSP64464.2024.10866240.

23. Rozov V.Y., Reutskiy S.Y., Pelevin D.Y., Kundius K.D. Magnetic field of electrical heating cable systems of the floors for residential premises. *Electrical Engineering & Electromechanics*, 2024, no. 5, pp. 48-57. doi: https://doi.org/10.20998/2074-272X.2024.5.07.

24. *Permanent neodymium magnets.* Available at: http://www.polus-n.com/post_magn_eng.html (Accessed: 22 July 2024).

25. *Finite Element Method Magnetics: Download – Stable Distribution (21Apr2019) – 64-bit Executable.* Available at: https://www.femm.info/wiki/Download (Accessed: 22 July 2024).

26. Rozov V.Y., Pelevin D.Y., Kundius K.D. Simulation of the magnetic field in residential buildings with built-in substations based on a two-phase multi-dipole model of a three-phase current conductor. *Electrical Engineering & Electromechanics*, 2023, no. 5, pp. 87-93. doi: https://doi.org/10.20998/2074-272X.2023.5.13.

27. Plesnetsov S.Y., Petrishchev O.N., Mygushchenko R.P., Suchkov G.M., Sotnik S.V., Kropachek O.Y. Powerful sources of pulse high-frequency electromechanical transducers for measurement, testing and diagnostics. *Electrical Engineering & Electromechanics*, 2018, no. 2, pp. 31-35. doi: https://doi.org/10.20998/2074-272X.2018.2.05.

Received 29.12.2024
Accepted 14.02.2025
Published 02.07.2025

V.F. Bolyukh[1], *Doctor of Technical Science, Professor,*
G.M. Suchkov[1], *Doctor of Technical Science, Professor,*
R.P. Mygushchenko[1], *Doctor of Technical Science, Professor,*
M.E. Kalnytskyi[1], *Postgraduate Student,*
[1] National Technical University «Kharkiv Polytechnic Institute»,
2, Kyrpychova Str., Kharkiv, 61002, Ukraine,
e-mail: vfbolyukh@gmail.com (Corresponding Author)

How to cite this article:
Bolyukh V.F., Suchkov G.M., Mygushchenko R.P., Kalnytskyi M.E. Determination of parameters of an autonomous source of a constant magnetic field for a portable electromagnetic-acoustic transducer. *Electrical Engineering & Electromechanics*, 2025, no. 4, pp. 72-79. doi: https://doi.org/10.20998/2074-272X.2025.4.09